

2016-01-0827

Reduction of Cold-Start Emissions through Valve Timing in a GDI Engine

Author, co-author (Do NOT enter this information. It will be pulled from participant tab in MyTechZone)

Affiliation (Do NOT enter this information. It will be pulled from participant tab in MyTechZone)

Abstract

This work examines the effect of valve timing during cold crank-start and cold fast-idle (1200 rpm, 2 bar NIMEP) on the emissions of hydrocarbons (HC) and particulate mass and number (PM/PN). Four different cam-phaser configurations are studied in detail: 1. Baseline stock valve timing. 2. Late intake opening/closing. 3. Early exhaust opening/closing. 4. Late intake phasing combined with early exhaust phasing. Delaying the intake valve opening improves the mixture formation process and results in more than 25% reduction of the HC and of the PM/PN emissions during cold crank-start. Early exhaust valve phasing results in a deterioration of the HC and PM/PN emissions performance during cold crank-start. Nevertheless, early exhaust valve phasing slightly improves the HC emissions and substantially reduces the particulate emissions at cold fast-idle. The combined strategy consisting of late intake and early exhaust phasing shows a considerable reduction in both the cold crank-start HC and PM/PN emissions of 30%. In fast idle, the HC and PM emissions respond differently to the different valve timing strategy. The combined late IVO and early EVC configuration with moderate combustion phasing retard gives the best HC and PM emissions and reasonable engine stability.

Introduction

Gasoline direct injection (GDI) engines have been rapidly adopted in the markets during the past decade, going from virtually 0% to a 38% market share in the US [1] and over 30% in the EU [2]. GDI engines have a number of advantages for reducing fuel consumption; however, the direct liquid injection poses some emissions challenges, especially for HC and PM during the cold-start phase. Figure 1 shows the tailpipe HC and PM/PN emissions during the FTP-75 for two representative GDI engines [3, 4]. In the representative case of Fig. 1, the cold-start phase is responsible for 97% of the HC emissions and 77% of the PM/PN emissions.

During cold-start, the combustion chamber walls are at a lower temperature than the saturation temperature of most of the fuel species; the result is the formation of fuel films which fail to completely evaporate prior to combustion. The fuel that does manage to evaporate from the spray and the films could form overly rich regions due to incomplete mixing; these regions are responsible for the high levels of HC and PM/PN emissions during cold-start. Additionally, the cold temperature increases the solubility of gaseous fuel into the oil layer prior to combustion. After combustion, the higher burned gas temperature and the low HC content of the burned gases favors desorption of the fuel back into the bulk gases, thereby providing an

additional source for HC emissions. The low piston temperature also results in larger crevice volumes, increasing the amount of gaseous fuel escaping combustion. Lastly, the post-flame oxidation rates of the HC that managed to escape the main combustion event, and of the particles formed during combustion, are reduced due to increased heat transfer from the bulk gases to the cold cylinder walls.

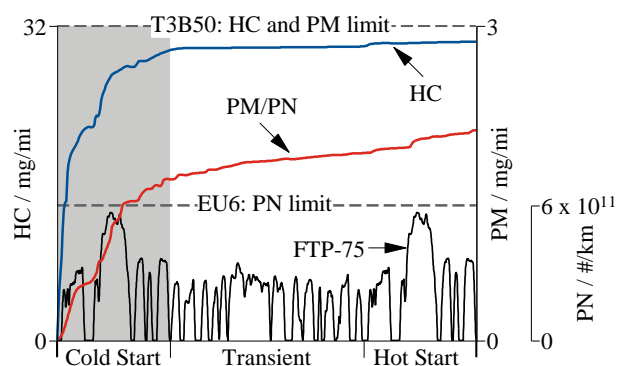


Figure 1. Cumulative tailpipe HC and PM/PN emissions over the FTP-75 cycle for GDI engines. The HC data correspond to a 2010 vehicle equipped with a 3.5 liters turbocharged GDI engine and a low temperature TWC [3]. The PM/PN data correspond to a 2.4 liters naturally aspirated GDI engine without a GPF [4]. The HC limit of T3B50 assumes the same HC/NO_x ratio as the T2B5 standard

This study is part of a wider effort undertaken at MIT to understand and mitigate the engine-out HC and PM/PN emissions during the cold-start phase [5, 6, 7, 8, 9]. This paper builds upon the findings and methodology of two previous studies on the 1st cycle emissions and fuel pathway during cold cranking [5, 6]. Additionally, it complements previous studies on emissions control through valve overlap [7], and through injection strategy [8, 9].

The goal of the present study is to quantify the potential of unconventional valve timing with large negative valve overlap (NVO) for reducing the engine-out HC and PM emissions during the cold crank-start and fast-idle phases of a GDI engine. With variable valve timing (VVT) systems, the selection of the de-energized position (parked position) of the camshafts is limited by the authority of the phasing system and the desired maximum intake advance and exhaust retard during warm operation. As the authority of VVT systems increases, new camshaft parked positions become possible. The merits of these parked positions for cold-start emissions control are discussed in this paper.

Experimental Methodology

Engine set up

The experimental study was carried out in a production 4 cylinder, 2 liter turbocharged GDI engine, featuring a centrally mounted spark plug, 4 valves per cylinder and a side mounted injector (see Table 1). The electromagnetic injectors have 6 holes each, an inclination of 25° respect to the horizontal, and a cone angle of 52°. The VVT system is hydraulically actuated, has an authority of 50°CA on each camshaft and allows the advancing of the intake valve timing and the retarding of the exhaust valve timing. For the investigations of delayed intake timing and advanced exhaust timing, the parked position of the camshafts had to be mechanically modified. The new parked positions of the camshafts were achieved by rotating the camshaft by 2 cam sprockets teeth. Since the cam sprockets have 46 teeth, a rotation of 2 teeth corresponds to a change in camshaft timing of approximately 31°CA.

Table 1. Specifications of the GM – LNF engine

Displacement	1998 cc
Bore / Stroke	86 / 86 mm
Connecting Rod	145.5 mm
Compression ratio	9.2:1
Fuel pressure	50 bar
Baseline inlet Valve Open / Close	11°aTDC / 61°aBDC @ 0.2 mm lift
Baseline max. intake valve lift	10.3 mm @ 126°aTDC _{intake}
Baseline exhaust Valve Open / Close	52°bBDC / 10°bTDC @ 0.2 mm lift
Baseline max. exhaust valve lift	10.3 mm @ 121°bTDC _{intake}

The fuel pressure was maintained at 50 bar using a hydro-pneumatic accumulator using nitrogen. This allows the fuel pressure to be set independently from engine speed, especially during cranking. The fuel used was a Tier II EEE certification gasoline with a carbon mass fraction of 86.5%, and 29% aromatics content. The fuel's RON and MON were 96.6 and 88.5 respectively. The Reid vapor pressure was 62.7 kPa with the distillation curve is shown in Fig. 2. The cold-start conditions were maintained by 3 independent chillers for the fuel, intake air, engine oil and coolant, maintaining all temperatures as close to 20°C as possible.

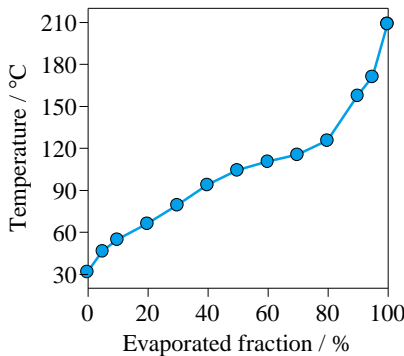


Figure 2. Distillation curve of the Tier II EEE certification gasoline used in the study

The exhaust composition was measured at the exhaust runner of cylinder 4 using fast response analyzers from Cambustion. The HC mole fraction was measured using an FFID unit, with a response time t_{10-90} of 1 ms, and a sampling position 8 cm from the exhaust valve. The CO and CO₂ mole fractions were measured with a fast NDIR unit, with a response time t_{10-90} of 8 ms, and a sampling position 6 cm from the exhaust valve. The PM and PN concentrations were measured using a fast particle spectrometer with a t_{10-90} of 300 ms, and a sampling point 15 cm from the exhaust valve. Additionally, the temperature and pressure of the working fluids were monitored at several positions. The locations of the different sensors are shown in Fig. 3.

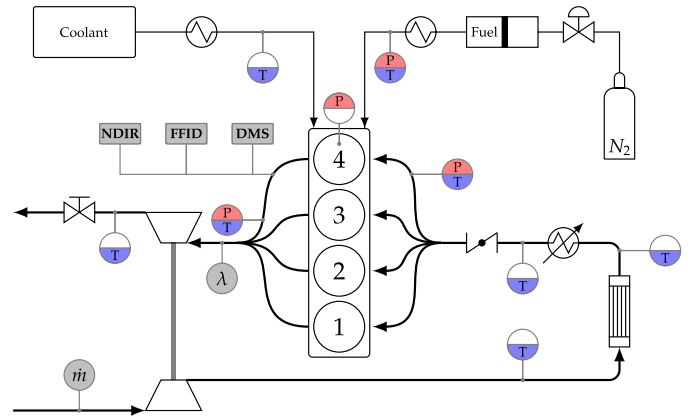


Figure 3. Diagram of the experimental setup and the sensor locations

The results presented in this paper deal with mass emissions of the aforementioned pollutants. The methodology to convert the mole fraction and concentration values to mass emissions is described in detail in a previous publication by the authors [5].

Experimental conditions

For this study four different valve timing were investigated, corresponding to the different combinations of exhaust timing advance and intake timing retard, as shown in Fig. 4. The experimental matrix with the resulting valve timings is shown in Table 2.

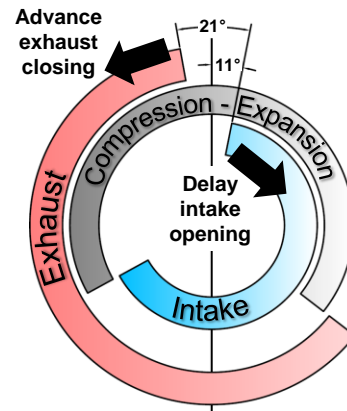


Figure 4. Baseline intake and exhaust timings and direction of phasing for the other investigated valve timings

Table 2. Experimental matrix

Case name	Intake timing @0.2mm lift	Exhaust timing @0.2mm lift
Baseline	IVO=11°CA aTDC IVC=61°CA aBDC	EVC=10°CA bTDC EVO=52°CA bBDC
Late IVO	IVO=42°CA aTDC IVC=92°CA aBDC	EVC=10°CA bTDC EVO=52°CA bBDC
Early EVC	IVO=11°CA aTDC IVC=61°CA aBDC	EVC=41°CA bTDC EVO=83°CA bBDC
Symmetric NVO (crank-start)	IVO=42°CA aTDC IVC=92°CA aBDC	EVC=41°CA bTDC EVO=83°CA bBDC
Symmetric NVO (fast-idle)	IVO=37°CA aTDC IVC=87°CA aBDC	EVC=36°CA bTDC EVO=78°CA bBDC

In order to cover the complete cold-start, two different sets of tests were carried out for this study: Cold crank-start and cold fast-idle.

To separate the effects of valve timing on the cold crank-start emissions from other parameters, the injected fuel mass for each cycle was adjusted to result in a similar combustion lambda during crank-start for all valve timing cases (see Fig. 5). The combustion lambda was calculated based on the CO and CO₂ mole fractions and disregarding the HC content [10]. Thus, the value represents the air equivalence ratio of the burned mixture. The spark timing for each cycle was adjusted for the initial 3 cycles, so that the point for 50% of heat release (CA50) was at a similar location for all valve timing cases studied. From the fourth cycle on, the spark timing was held constant for the rest of the crank-start process, resulting in later combustion phasing as the engine speed increased (see Fig. 5). For each valve timing setting, the throttle position was fixed throughout the cranking process at a position resulting in 2bar NIMEP at 1200 rpm (fast-idle conditions). For each experimental case, the injection timing was adjusted individually for the first three cycles and was chosen to minimize HC and PM emissions. From the 4th cycle on, the injection event took place during the mid-intake stroke (SOI=105°CA aTDC_{intake}) for all cases. Each experimental condition was repeated 5 times, and the results reported correspond to the average values.

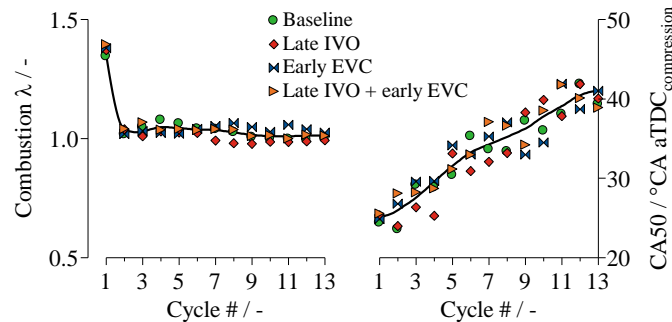


Figure 5. Combustion lambda and CA50 during the crank-start process for all four valve timings studied

Fast-idle engine management is an important part of the emissions control strategy during the cold start phase. During this quasi-steady period after crank-start, there should be sufficient exhaust enthalpy flow for a rapid warm-up of the TWC, while at the same time, maintaining low levels of pollutant emissions since the catalyst is not yet effective. For each valve timing case, the fast-idle experiments were carried out at a representative operating point summarized in Table 3. For the symmetric NVO case, the fast-idle valve timing differs

from the one at crank-start (see Table 2) due to stability issues (see section on Fast Idle Results later).

Table 3. Fast idle condition

Engine speed	1200 rpm
NIMEP	2 bar
Lambda	1
External EGR	0 %
Coolant, oil and fuel temperature	20 °C
Start of injection timing	105°CA aTDC intake
Intake temperature	20°C
Fuel pressure	50 bar
Nominal number of cycles	150 cycles

Cold crank-start results

Crank-start with late intake valve opening/closing

The delayed intake valve timing has beneficial effects on the mixture preparation process in GDI engines at cold temperature. With intake timing delayed, the intake valves remain closed during the initial part of the intake stroke and produces a drop in cylinder pressure. Thus, the pressure differential across the valve at IVO increases, resulting in higher air velocity and increased turbulence during the initial portion of the intake stroke [11, 12, 13]. These flow features promote fuel-air mixing. Figure 6 shows the cycle simulation results for the air velocity at the intake valve with different IVO timings. Compared to the baseline, the peak air velocity can increase up to 8 times for the latest IVO studied; note that the maximum velocity is limited by the choked flow condition.

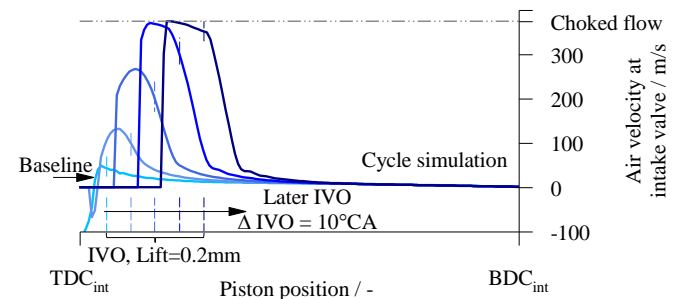


Figure 6. Air velocity through valve during the intake stroke as a function of IVO timing; cycle simulation results.

The cylinder pressure drop created in the intake stroke with late IVO timings also has a direct impact on the fuel spray evaporation. With the decrease in cylinder pressure, the potential for flash-boiling of the more volatile fraction of the fuel increases, thereby improving the spray breakup and aiding the spray evaporation and the mixture formation process [15, 16]. Figure 7 (right) shows the saturated vapor pressure at 25°C (calculated with the Antoine equation parameters from NIST [14]) for the main fuel species of a certification gasoline (UTG-91); the bubble size represents the volumetric fraction of the species in the fuel. As shown in Fig. 7 (left), a delay in IVO of 40°CA results in a minimum pressure of 300mbar for the first engine cycle during crank-start; this pressure is below the saturation pressure of all the C4 and C5 content of the fuel. Of particular relevance are the

species Isopentane (4.4 %^{vol}, $P_{sat} = 0.91$ bar), N-Pentane (1.4 %^{vol}, $P_{sat} = 0.68$ bar) and Cyclopentane (4.3 %^{vol}, $P_{sat} = 0.42$ bar) as together they represent 10% of the fuel content and their saturation pressures at ambient temperature are in the range achievable by the late IVO setting. It is worth pointing out that the minimum in-cylinder pressure is attained during the first half of the intake stroke. Thus, a fuel injection event during the minimum pressure region might result in substantial piston impingement which offsets the advantages of improved evaporation through flash-boiling.

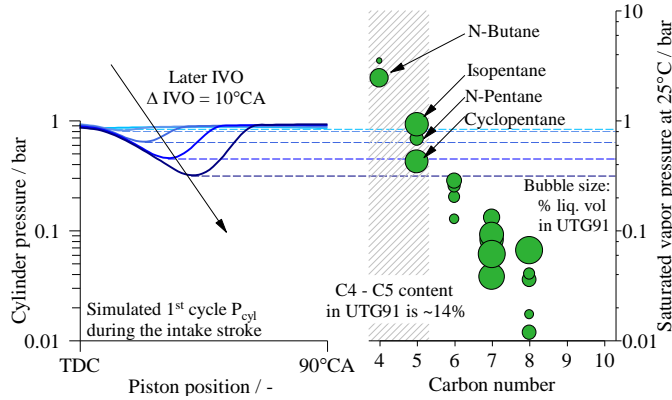


Figure 7. Left: Simulated in-cylinder pressure during intake stroke for the first engine cycle and different IVO timings. Right: Saturated vapor pressure at 25°C of the main constituents of the certification gasoline UTG-91

Retarding intake timing also results in higher charge temperature at the end of the intake stroke. The temperature increase facilitates the vaporization process. The increase in charge temperature is a result of the flow work in the cylinder filling process. To illustrate this, consider the extreme scenario of filling a completely evacuated rigid adiabatic cylinder with an ideal gas. The 1st law of thermodynamics for this system becomes:

$$\frac{d}{dt}(mc_v T)_{cyl} = \dot{m}c_p T_{amb} \quad (1)$$

Integrating from valve open to when pressure reaches equilibrium, the final cylinder temperature is a factor of γ higher than the ambient temperature:

$$T_{f,cyl} = \frac{c_p}{c_v} T_{amb} = \gamma T_{amb} \quad (2)$$

Therefore, the higher the mass inflow to equilibrate the pressure before the charge induction by the displacement process, the more flow work is done. Hence the overall trapped charge temperature increases with late IVO.

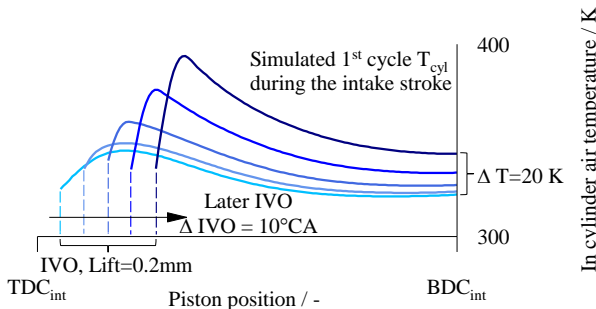


Figure 8. Simulated in-cylinder temperature during the intake stroke for the first engine cycle and different IVO timings

The above effect is illustrated in Fig. 8, which shows the result of a cycle simulation for the charge temperature throughout the intake stroke of the 1st engine cycle during crank-start. Retarding the IVO event 40°CA results in an increase in 20°C at the end of the intake stroke. The same increase in fuel temperature would approximately double the saturated vapor pressure of the different fuel species.

To experimentally test the effect of late IVO, the intake valve timing was delayed by 31°CA by rotating the intake camshaft 2 cam-sprocket teeth from the baseline. The resulting valve timing is shown in Fig. 9.

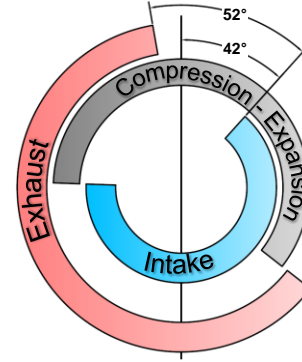


Figure 9. Valve timing diagram for the late IVO/IVC setting

Figure 10 (bottom) shows the required mass of fuel for the 1st cycle as a function of the λ of combustion for both the baseline valve timing and the late IVO setting. For the 1st combustion event during cold crank-start, the target combustion lambda is between 1.2 and 1.4; leaner mixtures increase the risk of partial burn or misfire, while lambda values closer to 1 result in locally fuel rich pockets responsible for significant CO production (Fig. 10, top). As discussed previously in this section, the late IVO facilitates fuel evaporation so that for a given combustion lambda in the window of interest, the late IVO case results in approximately a 13% reduction in fuel requirement.

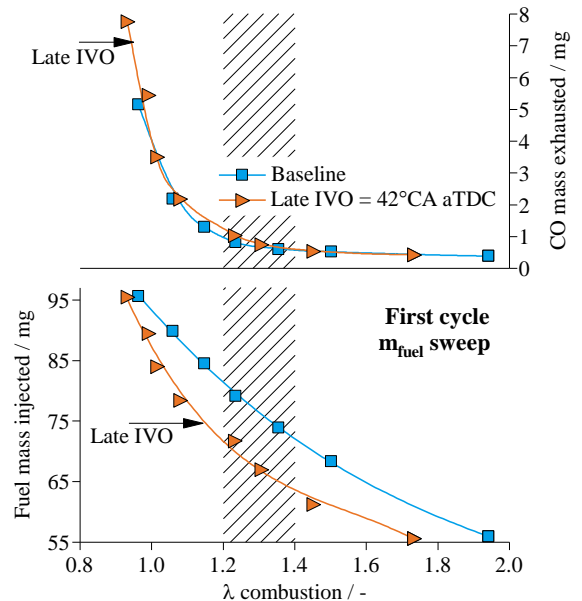


Figure 10. CO production (top) and 1st cycle fuel requirement (bottom) as a function of combustion lambda for baseline and late IVO settings

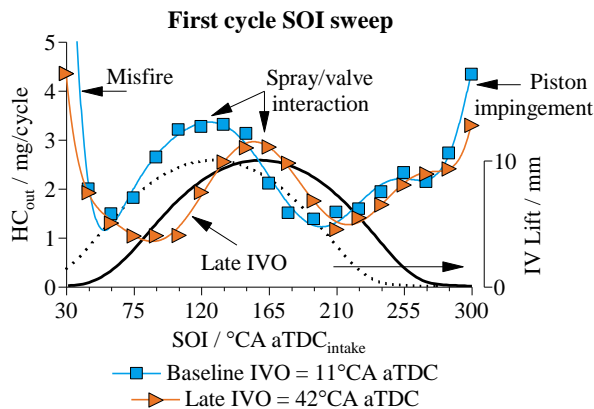


Figure 11. 1st cycle HC emissions as a function of SOI for both baseline and late IVO cases

In a previous study of the 1st cycle cranking process [5], it was found that, in order to avoid both piston and intake valve interactions with the spray, the optimum injection strategy for lowest 1st cycle emissions consists of a single injection event during the early compression stroke. As the IVO timing is delayed, the interaction zone between the fuel spray and the intake valve is shifted to a later point in the intake stroke; see Fig. 11. This shift enables injection during the first half of the intake stroke without interfering with the intake valve so that fuel bounce to the cylinder head is reduced. The latter is a major cause of the HC emissions for early injection (the high HC emissions region at the left-hand-side of Fig. 11). Thus in Fig. 11, which shows the results of a SOI sweep for both the baseline and late IVO cases at constant fuel mass, the SOI for lowest HC emissions is shifted from 195°C aTDC_{intake} for the baseline case, to 105°C aTDC_{intake} for late IVO, and the minimum HC emissions change from 1.5 to 1 mg/cycle.

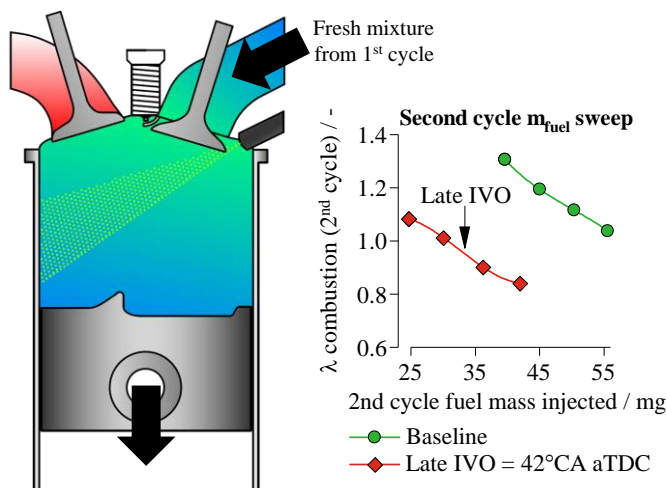


Figure 12. Mixture formation process during the 2nd cycle

With the IVO timing retard, the IVC timing is shifted to the mid-compression stroke. Consequently, part of the fresh mixture formed during the 1st engine cycle is pushed into the intake manifold, and is available for the 2nd cycle (see Fig. 12). As a result, the required mass of direct injected fuel for a given combustion lambda is reduced, diminishing the formation of fuel films during the 2nd cycle.

Figure 13 and 14 show the first 2 seconds of the cold crank-start, encompassing the period between the start of cranking till the maximum engine speed is achieved (speed flare), for both the baseline and late IVO cases. Fig. 13 (left) shows that the late IVO setting results in lower NIMEP for the first 2 engine cycles and consequently, results in a slower engine speed run-up and reduced speed-flare (Fig. 13, right). This observation is a consequence of the reduced trapped mass and lower ECR (effective compression ratio) resulting from late IVC. As the intake manifold is pumped down by the engine, the manifold pressure decreases more rapidly in the baseline case due to the narrower throttle opening necessary to achieve 2 bar of NIMEP at steady state. After the 3rd engine cycle, however, the lower cylinder volumetric efficiency of the late IVO setting is compensated for by the wider throttle opening. Then for both valve timings, comparable NIMEP traces are obtained.

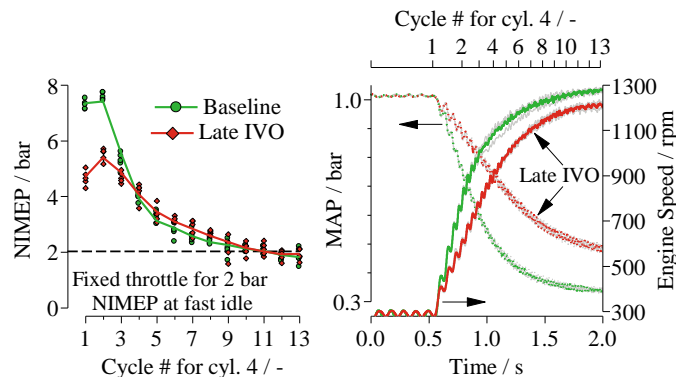


Figure 13. NIMEP, engine speed and MAP traces during cold crank-start for baseline and late IVO. Symbols are for individual run results; colored lines represent average values of 5 separate runs

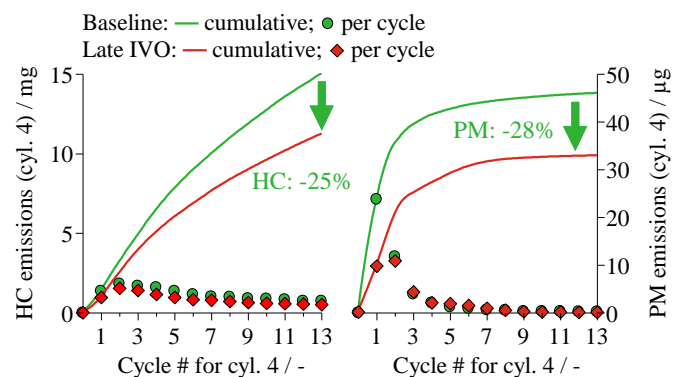


Figure 14. Cycle-by-cycle and cumulative HC and PM emissions of cylinder 4 during cold crank-start for the baseline and late IVO settings

Regarding the engine out emissions, Fig. 14 shows the HC and PM traces during cold crank-start. The general trends for both valve timing settings are as follows. The HC emissions peak at the 2nd cycle and approach a steady-state value between 0.3 - 0.5 mg/cyl./cycle. As the crank-start progresses, the reduction in HC is caused by better mixture formation driven by the increase in engine speed and in cylinder wall temperature. The PM emissions show a similar trend, peaking at the 1st or 2nd cycle, and approaching a steady-state value between 0.015 - 0.04 µg/cyl./cycle. PM formation is a complex process with competing processes of nucleation, agglomeration and oxidation [17]. As the engine speed increases there is better mixing and less time available for fuel vapor pyrolysis, post-flame agglomeration and particle coagulations; thus the particulate emissions are reduced [18].

As discussed at the beginning of this section, compared to the baseline, the late IVO setting results in a reduction in HC emissions of 25%, both on a cycle-by-cycle basis, as well as cumulatively (Fig. 14 – left). In contrast, the 28% reduction in cumulative mass emissions of particulates during the initial 13 cycles for the late IVO setting is mainly attributed to the reduction in the 1st cycle PM emissions, while the subsequent cycles show comparable PM emissions for both cases.

Crank-start with early exhaust valve opening/closing

Advancing the exhaust valve timing has a direct impact on the residual gas fraction and the charge temperature during crank-start. When the EVC timing is advanced, the effective portion of the exhaust stroke is reduced, thereby increasing the amount of exhaust gas trapped at the end of the stroke. As the residual gas fraction increases, so does the charge temperature at the end of the intake stroke. Figure 15 shows the results of a cycle simulation at cranking speed for different values of exhaust valve advance; the results are representative of the conditions at the beginning of the 2nd engine cycle. As the EVC is advanced from the baseline to position to a maximum of 40°C CA, the residual gas fraction increases from 10% to 25%. The resulting increase in charge temperature during the intake stroke, due to the higher residuals, is on the order of 100°C. Such a temperature increase has the potential to improve the fuel spray evaporation and to reduce the formation of fuel films on the cylinder walls and piston crown.

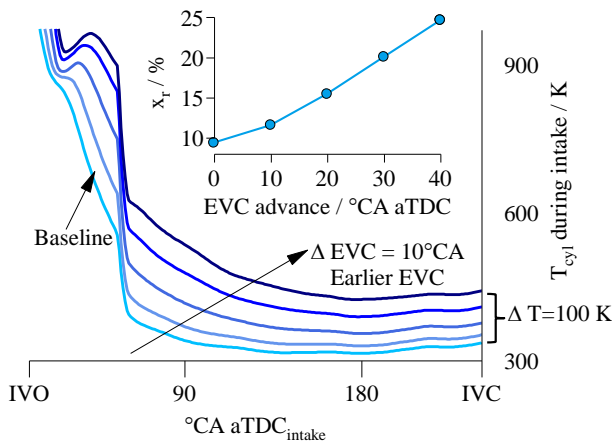


Figure 15. Simulated residual gas fraction and in-cylinder temperature during the intake stroke for the 2nd engine cycle and different EVC timings

To experimentally assess the potential benefits of early EVC, the exhaust valve timing was advanced by approximately 31°C CA by rotating the exhaust camshaft 2 cam-sprocket teeth from the baseline position. The resulting valve timing is shown in Fig. 16.

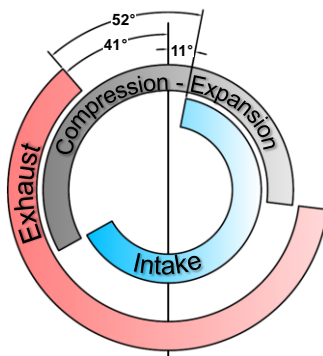


Figure 16. Valve timing diagram for the early EVO/EVC setting

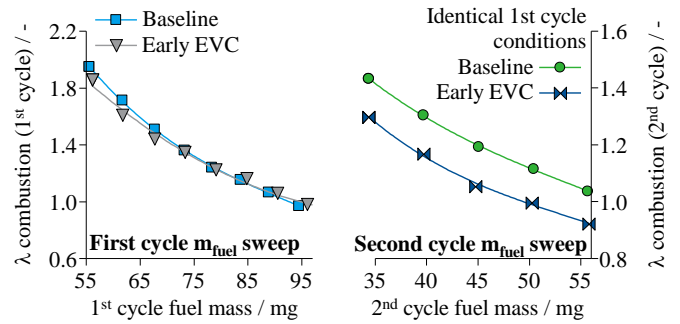


Figure 17. Baseline and early EVC results for the lambda of combustion as a function of the injected fuel amount for the 1st and 2nd engine cycles

The 1st engine cycle does not have residual gases. Thus the mixture formation process is not affected by the valve timing change (Fig. 17- left), and the dependence of the combustion lambda on the injected fuel mass is similar for both the baseline and the early EVC settings. For the 2nd cycle, however, the presence of residual gases results in a 15% lower fuel requirement for a given lambda of combustion. When the increase of residual gas fraction for the early EVC setting is accounted for (increasing from 9% in the baseline case to 22% in the early EVC setting), a 15% reduction in volumetric efficiency is expected. Therefore, the reduction in required fuel (for the same λ) is attributed to the air displacement by the residual gas. The greater residual gas fraction with early EVC does not play a significant role in the in-flight spray evaporation and mixture formation processes.

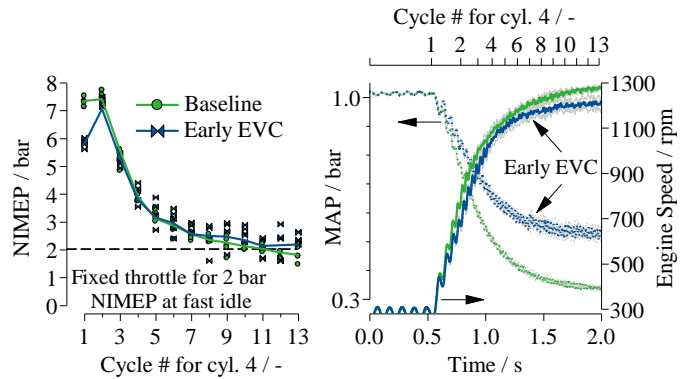


Figure 18. NIMEP, engine speed and MAP traces during cold crank-start for baseline and early EVC. Symbols are for individual run results; colored lines represent mean values of 5 separate runs

Figure 18 shows the first 2 seconds of the cold crank-start, between the start of cranking and the speed flare, for both the baseline and early EVC cases. For the first cycle, despite the similar mixture formation process (Fig. 17, left) and same intake manifold pressure during the intake stroke (Fig. 18, right), the early EVC setting resulted in lower NIMEP. This difference can be explained by the GIMEP loss associated with early EVO, and the increase in pumping losses caused by the early EVC (see Fig. 19, left). The impact of the lower 1st cycle NIMEP can be observed in the speed trace in Fig. 18, as the engine speed run-up is slightly slower during the first cycle, and that the speed-flare is reduced. As the engine speed increases and the intake manifold is pumped down, the early EVO/EVC work losses are compensated by the wider throttle opening, and the NIMEP traces are comparable after the 2nd engine cycle.

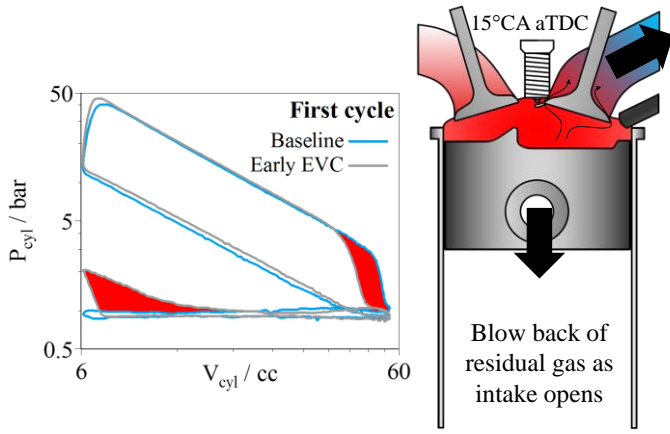


Figure 19. Work output losses caused by early EVO/EVC

The HC and PM cycle-by-cycle and cumulative emissions are shown in Fig. 20. Early EVC setting results in 20% and 48% increase in HC and PM cumulative emissions respectively. The 1st cycle HC and PM emissions are equivalent for both baseline and early EVC settings due to the absence of residual gases. From the 2nd cycle on, the increased internal EGR caused by early EVC starts to have an impact on the emissions behavior.

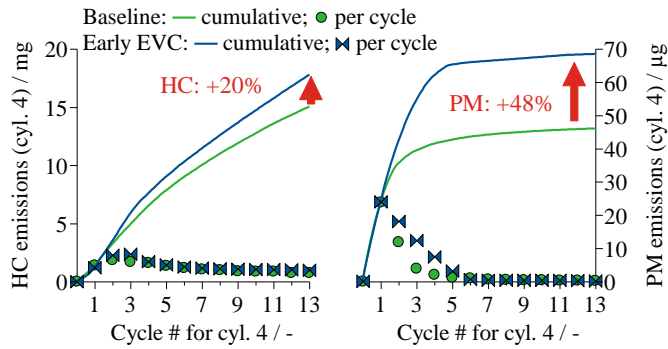


Figure 20. Cycle-by-cycle and cumulative HC and PM emissions of cylinder 4 during cold crank-start for the baseline and early EVC settings

With the early EVC, the increase in HC emissions may be attributed to the lower burned gas temperature (since the combustion phasing is kept the same; see Fig. 5 right) associated with the higher residual gas fraction; thus suppressing post-flame oxidation [19]. The lower burned gas temperature also renders the flame more easily quenched at the fuel rich pockets; thereby, larger regions of soot producing pyrolysis region are formed [9]. Hence PM emissions increase.

Crank-start with late intake and early exhaust phasing

The final valve timing strategy studied, referenced as symmetric NVO, is a combination of late IVO and early EVC. The intake valve timing was delayed by the same amount the exhaust valve timing was advanced. Each camshaft was rotated 31°CA (2 cam-sprocket teeth) from the baseline position in the respective direction. The resulting valve timing (Fig. 21) has a symmetric NVO of 83°CA.

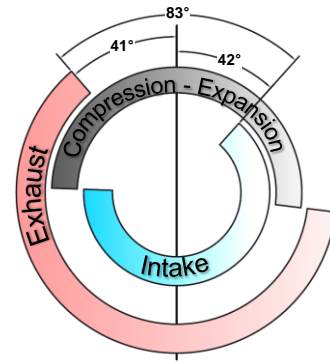


Figure 21. Valve timing diagram for the symmetric NVO strategy

With the symmetric NVO strategy there is an increase in residual gas fraction brought along by early EVC. The reduction in effective compression ratio due to late IVC and the reduction in effective expansion ratio due to early EVO have an impact in the work output of the first few engine cycles. For the later cycles, these effects are compensated for by the throttle setting which takes into effect as the MAP adjusts to the equilibrium value. In comparison to the early EVC strategy, the symmetric NVO setting reduces the blowback of the trapped residual gases, as the late IVO allows for the expansion of the residual gases prior to IVO.

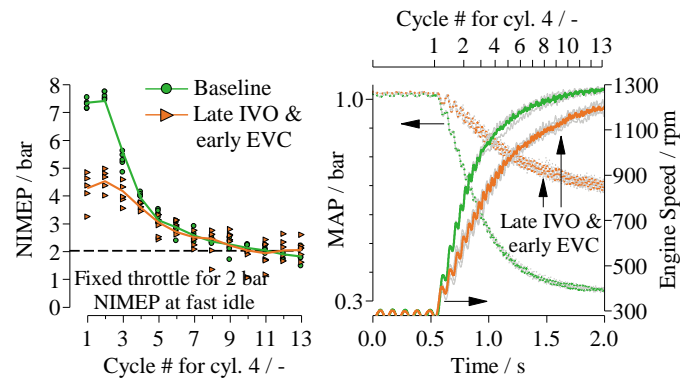


Figure 22. NIMEP, engine speed and MAP traces during cold crank-start for baseline and symmetric NVO. Symbols are for individual run results; colored lines are mean values of 5 separate runs

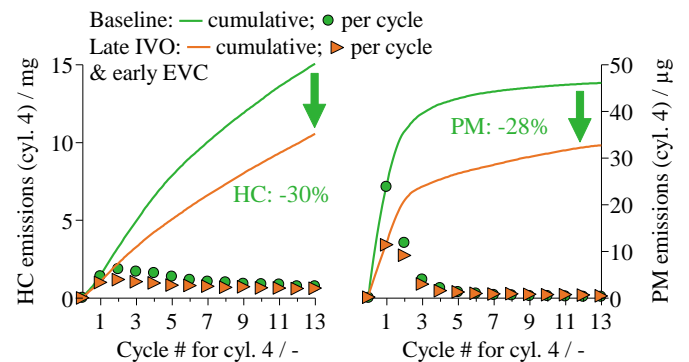


Figure 23. Cycle-by-cycle and cumulative HC and PM emissions of cylinder 4 during cold crank-start for the baseline and symmetric NVO settings

Figure 22 shows the progression of the cold crank-start during the first two seconds for the baseline and symmetric NVO cases. A sharp reduction in NIMEP is observed for the first three engine cycles of the symmetric NVO case. This is a result of the reduction in fresh mixture trapped at IVC (late IVO). The resulting speed trace resembles the late IVO case, with a reduced speed transient and flare. In order to achieve 2 bar NIMEP, a wider throttle position is required, resulting in a MAP value of 0.65 bar after 2 seconds (for comparison, ~0.3 bar for baseline and ~0.5 bar for late IVO or early EVC).

Figure 23 shows the cycle-by-cycle and cumulative HC and PM emissions for both baseline and symmetric NVO strategies. Comparing the symmetric NVO results to the previous two strategies discussed (late IVO: Fig. 14; early EVC: Fig. 20), the measurements show a greater resemblance to the emissions reduction achieved with late IVO, as the HC and PM cumulative emissions are reduced in 30% and 28% correspondingly with respect to the baseline. The reduction in HC emissions is more prominent during the first five engine cycles, with the difference becoming smaller as the crank-start progresses. As in the late IVO case, the reduction in PM stems mainly from the 1st cycle.

Fast-idle results

This section presents results of the fast-idle experiments. The cold fast-idle is a short quasi-steady period between the end of the crank-start and the first acceleration event in the certification cycle (20 seconds in the FTP-75 and 11 seconds in the NEDC). The operating condition used for studying this period is shown in Table 3. The objectives during the fast-idle are twofold: to provide a high thermal enthalpy flow to the TWC to facilitate light-off, and to keep the pollutant emissions low since the catalyst is not fully effective. The fast-idle experiments were carried out at the four different valve timings summarized in Table 2. Note that the symmetric NVO setting in the fast-idle experiments differs from the one used for the cold crank-start in the previous section by 10°CA of negative-overlap. The reduction in NVO at fast-idle was necessary to improve the engine stability with the late combustion phasing cases for the fast-idle study.

Combustion phasing has a significant impact on the fast idle HC [8] and PM [9] emissions. Figure 24 (a) and (b) shows the HC and PM emission indices (emission mass/fuel mass) for all the valve timings studied as a function of the combustion phasing which is quantified by CA50. In general, HC and PM emissions are reduced with delayed combustion phasing up to a certain point after which the emissions increase again with further combustion retard.

For HC emissions (as measured by the HC index defined as the HC mass/fuel mass), the reduction in peak pressure with retarded combustion reduces the in-crevice storage of unburned mixture. Higher post-flame and exhaust temperature increase the post-oxidation rate of the unburned HC. However, with very late combustion phasing, there may be incomplete combustion. These confounding factors result in the “hook” trend observed in Fig. 24 (a).

The decrease of the PM index (PM mass/ fuel mass) with retarded combustion is attributed to the increase in fuel vaporization and mixing because combustion occurs later. Hence, the fuel rich soot production region is reduced. The reduction of HC described in the last paragraph also decreases the HC condensation on the particulates. At very late combustion phasing, however, the increase in HC due to partial burn may lead to a higher PM value because of HC condensation on the particulates; see Fig. 24 (b).

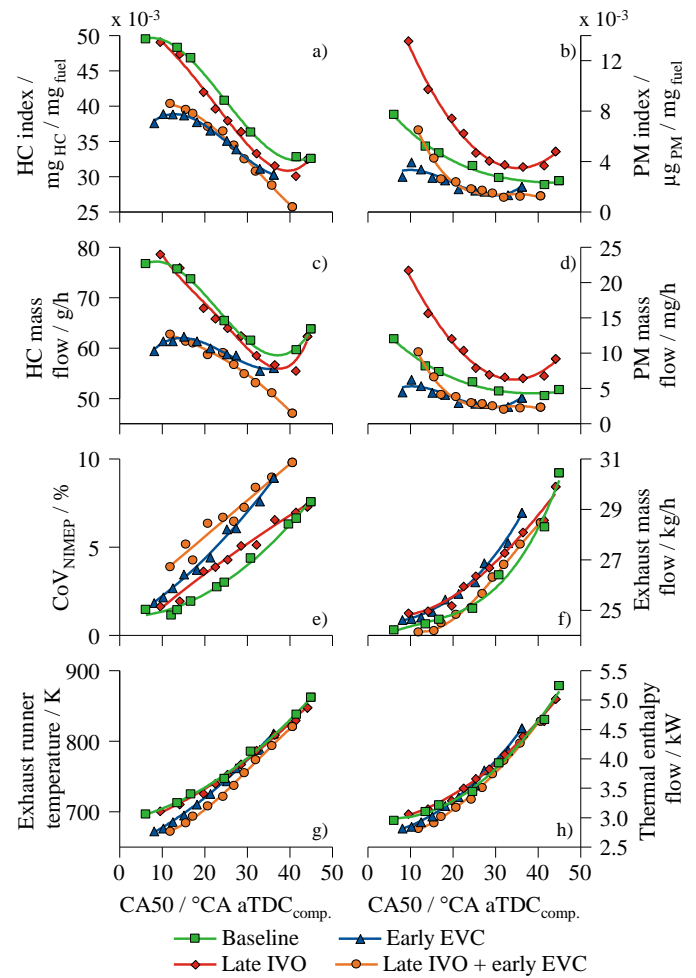


Figure 24. Results for the cold fast-idle experiments for all the valve timings studied. Combustion phasing (CA50) dependence of: a) HC emissions index (normalized to fuel mass). b) PM emissions index (normalized to fuel mass). c) HC mass flow. d) PM mass flow. e) CoV of NIMEP. f) Exhaust mass flow rate. g) Exhaust temperature (runner of cyl. 4). h) Thermal enthalpy flow.

The emissions quantities of interest are the emission flow rates which are the products of the emission indices and fuel flow rates. For a fixed λ , the fuel flow and total exhaust flow are proportional; the latter values are plotted in Fig. 24 (f). To compensate for the decrease in fuel conversion efficiency, the fuel and hence exhaust flows (at constant λ) increase substantially with combustion retard. However, because of the large decrease in emission indices with retard, the overall effect is that emission flow rates still decrease with retard until at very late combustion phasing; see Fig. 24 (c) and (d).

Engine roughness is a concern with combustion phasing retard. The CoV of NIMEP are shown as a function of CA50 in Fig. 24 (e). For CA50 up to 45° CA aTDC-compression, the values are under 10% which is considered tolerable at fast idle. Combustion retard facilitates catalyst light-off by both increasing the exhaust temperature (Fig. 24 (g), which are values at 10 cm from the exhaust valve of cylinder #4), and exhaust flow rate (Fig. 24 (f)). The resulting thermal enthalpy flows are shown in Fig. 24 (h). The thermal enthalpy flow is in Eq. 3, with T_{ref} taken as 25°C. From CA50 = 7° (MBT timing) to CA50 = 45°CA aTDC-compression, the thermal enthalpy flow increases by 1.8 times.

$$\text{Thermal enthalpy flow} = \dot{m}_{exh} c_p (T_{exh} - T_{ref}) \quad (3)$$

The valve timing arrangements have different impacts on HC and PM emission flows; see Fig. 24 (c) and (d). For combustion retard with CA50 in the range of 30° – 40°CA aTDC-compression, which gives low emission flows, high enthalpy flow and reasonable CoV of NIMEP, the combination of late IVO plus early EVC gives the best results – compared to the baseline, the HC flow decreases by ~ 10 – 25%, and the PM flow decreases by ~50%.

Conclusions

The effects of four valve timing settings on the cold-start HC and PM emissions during crank-start and fast-idle were studied in a wall guided gasoline direct injection engine. The valve timings examined were the stock position, late IVO, early EVC and a combination of the last two, dubbed symmetric NVO. The following conclusions are drawn.

In the cold-start cranking process:

1. Late IVO improves the mixture formation process in cold crank-start and reduces the exhaust mass flow during the critical 1st cycle exhaust event. The delayed intake timing results in 25% and 28% reduction of the cumulative HC and PM cold crank-start emissions respectively.
2. Early EVC results in a deterioration of the HC and PM/PN emissions in cold crank-start. The increase in cumulative emissions comprises mainly the contributions from the early cycles (2nd through 5th). (The EVC timing does not have any effect on the 1st cycle which has no residual.)
3. The combined strategy consisting of late intake and early exhaust phasing shows a reduction in the cumulative crank-start HC and PM/PN emissions similar in magnitude and cycle-to-cycle progression to the late IVO case. Thus early EVC has less impact on the crank-start emissions compared to late IVO.

In the cold fast-idle process (exemplified by the operating point of 1200 rpm, 2 bar NIMEP, and 20° C ECT):

4. Significant decreases of both HC and PM emission indices (emission mass/fuel mass) are observed with retard in combustion phasing. At very late phasing, the emissions go up again.
5. The above decrease in emissions over-powers the increase in engine through-put rate (to maintain same NIMEP, since the fuel conversion efficiency is lower with retard combustion) so that the HC and PM exhaust flow rate decreases with combustion retard until very late phasing is reached.
6. The response of HC and PM emission flows to valve timing are different. For retarded combustion with CA50 in the range of 30° to 40°CA aTDC-compression, which gives low emission flows, high enthalpy flow and reasonable CoV of NIMEP, the symmetric NVO case gives the best results – compared to the baseline timing, the HC flow decreases by 10-25% and the PM flow decreases by ~50%.

References

1. Davis, Stacy, Susan Diegel, Ridge Boundy, and Sheila Moore. "Vehicle Technologies Market Report 2014." Oak Ridge National Laboratory, 2015

2. "European Vehicle Market Statistics, 2014." International Council on Clean Transportation, 2014.
3. Chen, Hai-Ying, and Hsiao-Lan (Russell) Chang. "Development of Low Temperature Three-Way Catalysts for Future Fuel Efficient Vehicles." *Johnson Matthey Technology Review* 59, no. 1 (January 1, 2015): 64–67. doi:10.1595/205651315X686011.
4. Myung, Cha-Lee, Juwon Kim, Wonwook Jang, Dongyoung Jin, Simsoo Park, and Jeongmin Lee. "Nanoparticle Filtration Characteristics of Advanced Metal Foam Media for a Spark Ignition Direct Injection Engine in Steady Engine Operating Conditions and Vehicle Test Modes." *Energies* 8, no. 3 (March 9, 2015): 1865–81. doi:10.3390/en8031865.
5. Rodriguez, J. Felipe, and Wai K. Cheng. "Effect of Operation Strategy on First Cycle CO, HC, and PM/PN Emissions in a GDI Engine." *SAE International Journal of Engines* 8, no. 3 (April 14, 2015). doi:10.4271/2015-01-0887.
6. Rodriguez, J. Felipe, and Wai K. Cheng. "Fuel Carbon Pathway in the First Cranking Cycle of a Gasoline Direct Injection Engine." *International Journal of Engine Research*, October 5, 2015. doi:10.1177/1468087415609852.
7. Cedrone, Kevin, and Wai K. Cheng. "Using Valve Timing and Exhaust Back Pressure to Improve Catalyst Warm-Up Time," SAE Technical Paper 2013-01-2656, 2013. doi:10.4271/2013-01-2656.
8. Cedrone, Kevin, and Wai K. Cheng. "SI Engine Control in the Cold-Fast-Idle Period for Low HC Emissions and Fast Catalyst Light Off." *SAE International Journal of Engines* 7, no. 2 (April 1, 2014): 968–76. doi:10.4271/2014-01-1366.
9. Ketterer, Justin E., and Wai K. Cheng. "On the Nature of Particulate Emissions from DISI Engines at Cold-Fast-Idle." *SAE International Journal of Engines* 7, no. 2 (April 1, 2014): 986–94. doi:10.4271/2014-01-1368.
10. Silvis, William M. "The Algorithmic Structure of the Air/Fuel Ratio Calculation." *Readout HORIBA Technical Reports* 15 (1997): 17–24.
11. Lang, Kevin R., Wai K. Cheng, Mark Borland, Chris Thomas, and Fuquan Zhao. "Effect of Intake Cam Phasing on First Cycle Fuel Delivery and HC Emissions in an SI Engine." SAE Technical Paper 2004-01-1852, 2004. doi:10.4271/2004-01-1852.
12. Roth, David, James Sisson, Marty Gardner, and Braman Wing. "Valve-Event Duration Reduction Through Ultra-Fast Phaser Actuation." SAE Technical Paper 2007-01-1281, 2007. doi:10.4271/2007-01-1281.
13. Sellnau, M., T. Kunz, J. Sinnamon, and J. Burkhard. "2-Step Variable Valve Actuation: System Optimization and Integration on an SI Engine." SAE Technical Paper 2006-01-0040, 2006. doi:10.4271/2006-01-0040.
14. Linstrom, P.J., and W.G. Mallard. *NIST Chemistry WebBook, NIST Standard Reference Database Number 69*. Gaithersburg MD, 20899: National Institute of Standards and Technology. Accessed June 6, 2015. <http://webbook.nist.gov>.
15. Schmitz, Ingo, Wolfgang Ipp, and Alfred Leipertz. "Flash Boiling Effects on the Development of Gasoline Direct-Injection Engine Sprays." SAE Technical Paper 2002-01-266, 2002. doi:10.4271/2002-01-2661.
16. Koga, Nobuhiko, Shigeki Miyashita, Keiso Takeda, and Nobuo Imatake. "An Experimental Study on Fuel Behavior During the Cold Start Period of a Direct Injection Spark Ignition Engine." SAE Technical Paper 2001-01-0969, 2001. doi:10.4271/2001-01-0969.
17. Haynes, B.S., and H.Gg. Wagner. "Soot Formation." *Progress in Energy and Combustion Science* 7, no. 4 (1981): 229–73. doi:10.1016/0360-1285(81)90001-0.

18. Hedge, Michael, Phillip Weber, Jess Gingrich, Terrence Alger, and Imad A. Khalek. "Effect of EGR on Particle Emissions from a GDI Engine." *SAE International Journal of Engines* 4, no. 1 (April 12, 2011): 650–66. doi:10.4271/2011-01-0636.
19. Heywood, John B. *Internal Combustion Engine Fundamentals*. New York: McGraw-Hill, 1988.

Contact Information

Felipe Rodríguez, jfrb@mit.edu

Wai Cheng, wkcheng@mit.edu

Acknowledgments

The authors would like to acknowledge the support for this research by Borg-Warner, Fiat Chrysler Automobiles, Ford Motor Company, and General Motors Company through a Consortium on Engine and Fuels Research.

Abbreviations

°CA	Crank Angle degree
AFR	Air Fuel Ratio
aTDC-c	After Top Dead Center Compression
aTDC-i	After Top Dead Center Intake
BDC	Bottom Dead Center
CA50	Point for 50% of heat release
CMD	Count Median Diameter
CoV	Coefficient of Variation

EVC	Exhaust Valve Closing
EVO	Exhaust Valve Opening
FFID	Fast Flame Ionization Detector
FTP	Federal Test Procedure
γ	Heat capacity ratio
GDI	Gasoline Direct Injection
GIMEP	Gross Indicated Mean Effective Pressure
GPF	Gasoline Particle Filter
IVC	Intake Valve Closing
IVO	Intake Valve Opening
MAP	Manifold Absolute Pressure
MFB	Mass Fraction Burned
NDIR	Non-Dispersive Infrared sensor
NEDC	New European Driving Cycle
NIMEP	Net Indicated Mean Effective Pressure
NVO	Negative Valve Overlap
SOI	Start of Injection
VVT	Variable Valve Timing
TWC	Three Way Catalyst
TDC	Top Dead Center